
Discover Generics
Cost-Effective CT & MRI Contrast Agents
FRESENIUS KABI
WATCH VIDEO

AJNR

This information is current as of June 26, 2025.

Influence of Perianeurysmal Environment on the Deformation and Bleb Formation of the Unruptured Cerebral Aneurysm: Assessment with Fusion Imaging of 3D MR Cisternography and 3D MR Angiography

Toru Satoh, Megumi Omi, Chika Ohsako, Atsushi Katsumata, Yusuke Yoshimoto, Shoji Tsuchimoto, Keisuke Onoda, Koji Tokunaga, Kenji Sugiu and Isao Date

AJNR Am J Neuroradiol 2005, 26 (8) 2010-2018
http://www.ajnr.org/content/26/8/2010

Influence of Perianeurysmal Environment on the Deformation and Bleb Formation of the Unruptured Cerebral Aneurysm: Assessment with Fusion Imaging of 3D MR Cisternography and 3D MR Angiography

Toru Satoh, Megumi Omi, Chika Ohsako, Atsushi Katsumata, Yusuke Yoshimoto, Shoji Tsuchimoto, Keisuke Onoda, Koji Tokunaga, Kenji Sugiu, and Isao Date

BACKGROUND AND PURPOSE: **Surface irregularity and bleb formation are anatomical factors that are associated with aneurysm rupture. The perianeurysmal environment has been proposed as one factor that may influence aneurysm morphology. We have developed a fusion imaging technique of 3D MR cisternography and angiography that allows clear visualization of an aneurysm and its environment. This technique may prove useful in further understanding of the natural history of intracranial aneurysms.**

METHODS: **Fusion images of 3D MR cisternography and angiography were reconstructed by a perspective volume-rendering algorithm from the volume datasets of MR cisternography, obtained by a T2-weighted 3D fast spin-echo sequence, and coordinated MR angiography, by a 3D time-of-flight sequence. On the fusion images, the anatomic relationship of an aneurysm to the perianeurysmal structures was assessed, and the influence of perianeurysmal environment on the deformation and bleb formation of the aneurysm was investigated.**

RESULTS: **Marked and minor deformation and bleb formation of the aneurysmal dome were found at the areas confronted or adjacent to a certain contact with perianeurysmal structures, including cranial nerves, brain parenchyma, cranial base bones, petroclinoidal dural folds, and dura mater.**

CONCLUSION: **Fusion images of 3D MR cisternography and angiography can depict the contact of an aneurysm with its perianeurysmal environment; this may provide an additional parameter in consideration for the natural history of cerebral aneurysms.**

Cerebral saccular aneurysms are initially rounded, berrylike outpouchings that arise at a branching site on the parent artery within the free subarachnoid space (1). With an enlargement of the aneurysmal dome, the aneurysms touch the intracisternal anatomical elements, including cranial nerves, bridging and surface veins, small arteries, and arachnoid trabecula. As the aneurysms grow to a certain size beyond the capacity of the surrounding subarachnoid space, they may come into contact with the juxtacisternal structures, such as the adjacent brain parenchyma, cranial base bone, dural folds, and dura mater. Intrinsic factors related to the initiation, growth, and rupture of cerebral aneurysms have been elucidated regarding the geometric angioarchitecture (2–8), pathologic fragility of the wall and the cellular mechanisms of degeneration and repair (9, 10), and intraaneurysmal flow dynamics (6, 7, 11–18). In addition, contact of the aneurysm with the surrounding intra- and juxtacisternal structures (perianeurysmal environment) may cause either cranial nerve symptoms by the adhesive compression or deformation and bleb formation of the aneurysmal dome by the limitation in spatial expansion; these extrinsic factors

Received December 8, 2004; accepted after revision March 1, 2005.

From the Departments of Neurological Surgery (T.S.) and Diagnostic Radiology (M.O., C.O.), Ryofukai Satoh Neurosurgical Hospital, Hiroshima, Japan; the Department of Neurological Surgery (A.K., Y.Y., S.T.), Onomichi Municipal Hospital, Japan; and the Department of Neurological Surgery (K.O., K.T., K.S., I.D.), Okayama University Graduate School of Medicine, Dentistry and Pharmacy, Okayama, Japan.

Presented in part at the 14th Annual Meeting of the Japanese Society for Detection of Asymptomatic Disease, July 1, 2005, Nagoya, Japan.

Address correspondence to Toru Satoh, Department of Neurological Surgery, Ryofukai Satoh Neurosurgical Hospital, 5-23-23 Matsunaga, Fukuyama, Hiroshima 729-0104, Japan (e-mail: ucsfbtrc@urban.ne.jp).

© American Society of Neuroradiology

may play a role in the growth and rupture of cerebral aneurysms (19, 20).

Assessment of the anatomic relationship between the outer wall configurations of the aneurysmal complex and the perianeurysmal environment on the 3D MR cisternography can provide useful information, not only in surgical or interventional treatments but also for investigating the natural history of unruptured cerebral aneurysms (20). In the present study, we have developed a fusion imaging technique of 3D MR cisternography and 3D MR angiography. The 3D MR cisternography–MR angiography fusion images were applied for the evaluation of the contact of unruptured cerebral aneurysms with their perianeurysmal environments.

Methods

Thirteen patients with unruptured cerebral aneurysms that were detected at MR angiography underwent MR cisternography; 5 aneurysms were located at the internal carotid artery, 2 at the anterior communicating artery, 3 at the middle cerebral artery, and 3 at the basilar artery. The patients' ages ranged from 54 to 83 years old (mean [±SD] 68.5 ± 8.1 years; 3 men; 10 women). Six patients underwent surgery, the others were followed-up, and 1 aneurysm ruptured in 14 months.

MR Cisternography Data Acquisition

MR cisternography was performed with a clinical MR imager (Signa HiSpeed 1.0T, General Electric Healthcare, Milwaukee, WI) using a T2-weighted 3D fast spin-echo sequence. We used the following parameters: TR/TE, 4000/160; number of excitations, 1; echo-train length, 128; bandwidth, 15.63 kHz; matrix, 256 × 256; section thickness, 0.6 mm; section interval, 0.6 mm; field of view, 16 cm; and total imaging time, 13 minutes 23 seconds. A total of 96 continuous source axial images were acquired. Volume data were transferred to an independent workstation with medical visualization software (Zio M900 Quadra, AMIN, Tokyo, Japan).

Reconstruction of Fusion Images of 3D MR Cisternography and MR Angiography

Data of MR cisternography were processed into the 3D volume-rendering dataset (84 data points) in 9 seconds. The 3D MR cisternogram was rendered from the data set in 11 seconds using a perspective volume-rendering algorithm. On the signal intensity histogram (arbitrary unit distribution) drawn on the source axial image of the MR cisternogram, the parent arteries, an aneurysm, the petroclinoidal dural fold and dura mater, and cranial base bone showed profoundly low signal intensity (50–100); juxtacisternal brain and cranial nerves, moderately low signal intensity (250–300); and surrounding cerebrospinal fluid, profoundly high signal intensity (500–750). To visualize the margin of the vessels, nerves, and brain parenchyma in 3D, we selected the entire area that was hypointense relative to cerebrospinal fluid from the opacity chart of the signal-intensity distribution using a function of a declining curve. The threshold value of this curve was adjusted according to each individual signal-intensity distribution pattern with a threshold range of 390–450 (100% opacity level), declining to 410–470 (0% opacity level, width 20), and color-rendered in blue. The 3D MR cisternogram depicted the spatial expansion of the contours of intracisternal objects in relation to the pericisternal structures and projected from various intracisternal viewpoints with a visual angle of 90°.

MR angiography was performed with the same scan baseline, and data were obtained using a 3D time-of-flight sequence, spoiled gradient-recalled acquisition in the steady state. We used the following protocol: TR/TE. 3.5/3.9-4.1; number of excitations, 2, flip angle, 20°; matrix, 192 × 128; section thickness, 1.2 mm; section interval, 0.6 mm; field of view, 16 cm; without magnetization transfer contrast; and total imaging time, 8 minutes 49 seconds (2 slabs), 120 sections in total (2 slabs); zero-fill interpolation processing 2 times; overlap of 8 sections. A total of 104 source images was obtained. Volume data were transferred to the same workstation. Data were interpolated every 0.6 mm and processed into 3D volume-rendering datasets. The 3D MR angiography was rendered using an increasing curve starting with a threshold of 155–175 (0% opacity level) and up to 165–185 (100% opacity level, width 10) and color-rendered in red.

A fusion image of 3D MR cisternography–MR angiography was reconstructed on a workstation by compositing 3D MR cisternography and its coordinated 3D MR angiography; each individual image was rendered from each volume-rendering dataset. To emphasize the vascular components, we used an MR angiography–weighted fusion image by compositing 3D MR cisternography (opacity level of 15%, in blue) and 3D MR angiography (100% opacity level, in red). Using reconstruction parameters of the function curves saved on the workstation, we instantly reproduced standard images of 3D MR cisternography, 3D MR angiography, and the fusion 3D MR cisternography–MR angiography; however, certain adjustments of the threshold range were needed to refine the contours of objects in each individual case. Total average time required to produce fusion images was approximately 30–50 seconds per image from postscanning.

Results

On the source axial images of MR cisternography, the aneurysmal complex and surrounding cisternal and pericisternal structures were depicted as negative shadows in contrast to the surrounding hyperintense subarachnoid cerebrospinal fluid. The 3D MR cisternogram showed the spatial relationship of an aneurysm and parent arteries to the adjacent bridging and surface veins, cranial nerves, tentorial free edge, petroclinoidal dural folds, dura mater, cranial base bone, and brain parenchyma in perspective views. With use of the 3D MR cisternography–MR angiography fusion image, we discriminated the vascular structures depicted on 3D MR cisternography by referencing the coordinated 3D MR angiography. Contact between the outer wall configuration of cerebral aneurysms and the anatomic elements of the perianeurysmal environment was assessed on the 3D MR cisternography, 3D MR angiography, and MR angiography–weighted 3D MR cisternography–MR angiography fusion images from various projections within a cisternal space. Image data of location and size of aneurysms (x, y, z), the maximum size of the parent artery, depth/neck width, aspect ratio, deformation and number of dome blebs, contact anatomical elements, and results are summarized in the Table.

Illustrative Cases

Case 1: Unruptured Internal Carotid-Posterior Communicating Artery Aneurysm (Fig 1)

A 75-year-old woman had a left internal carotid-posterior communicating artery aneurysm. The se-

Image data of incidentally discovered unruptured cerebral aneurysms

Patient No./ Age (y)/Sex	Aneurysm Site	Dome Size (x, y, z, mm)	Afferent Artery (mm)	Aneurysm Dome				Contact	Results
				Depth/Neck Width (mm)	Ratio of Depth/Neck	Degree of Deformation	No. of Blebs		
1/75/F	IC-PC	11.7 × 9.4 × 9.8	4.6	9.5/7.5	1.27	++	3	DS, CN-III, PF, TL	Follow-up
2/77/F	IC-PC	9.3 × 8.7 × 9.7	4.8	8.5/4.8	1.78	++	1	TL, CN-III	Follow-up
3/60/M	IC-PC	9.2 × 8.4 × 7.3	3.7	10.6/4.3	2.47	+	1	CN-III, TL	OP/CN-III Palsy
4/83/F	IC-PC	8.6 × 8.6 × 11.3	4.0	9.8/7.6	1.29	+	0	PF, TL	OP
5/58/M	IC-PC	2.9 × 2.9 × 4.5	4.3	2.3/4.7	0.49	++	1	TL	OP
6/54/M	AComA	5.4 × 4.4 × 5.8	3.3	3.6/4.7	0.77	+	1	FL	OP
7/76/F	AComA	4.4 × 4.5 × 4.1	3.0	3.4/3.1	1.10	+	1	ON, Chiasm	Follow-up
8/67/F	MCA	5.3 × 7.9 × 7.6	2.8	10/4.5	2.22	+	1	TL, SV	Follow-up
9/68/F	MCA	3.8 × 5.9 × 3.0	3.7	4.5/4.2	1.07	−	1	TL	OP
10/68/F	MCA	4.2 × 3.6 × 5.2	2.3	3.3/3.9	0.85	+	1	TL	OP
11/67/F	BA-Top	4.5 × 5.6 × 6.7	3.4	5.2/3.4	1.53	−	1	BS	Follow-up
12/70/F	BA-Top	7.3 × 10.6 × 5.6	6.6	10.2/6.4	1.59	++	2	DE	Ruptured
13/68/F	BA-AICA	2.7 × 2.7 × 3.8	2.9	2.7/3.3	0.82	−	1	BS	Follow-up

Note.—Content indicates contact of the dome with perianeurysmal structures; IC-PC, internal carotid-posterior communicating artery; AComA, anterior communicating artery; MCA, middle cerebral artery; BA-Top, top of basilar artery; BA-AICA, basilar artery-anterior inferior cerebellar artery; DS, dorsum sellae; CN-III, oculomotor nerve; PF, petroclioidal dural fold; TL, temporal lobe; FL, frontal lobe; ON, optic nerve; Chiasm, optic chiasm; SV, surface vein; BS, brain stem; DE, floor of the third ventricle (diencephalon).

lected maximum intensity projection image reconstructed from the source axial CT angiogram (Fig 1*A*), superoinferior projection, showed the aneurysmal complex and cranial base bone. The 3D CT angiogram (Fig 1*B*), posteroanterior projection, showed the aneurysm, posterior communicating artery, posterior clinoid process, and petroclinoidal dural fold. The selected minimum intensity projection image reconstructed from the source axial MR cisternogram (Fig 1*C*), superoinferior projection, depicted the aneurysmal complex, posterior clinoid process and dorsum sellae, petroclinoidal dural fold, and the adjacent temporal lobe. The 3D MR cisternogram (Fig 1*D*), obtained using a projection similar to that of the CT angiogram and viewed from the basal cistern, showed the spatial expansion and contact of the aneurysm with the perianeurysmal structures. The left oculomotor nerve ran downward to the posterior margin of the posterior clinoid process and forward over the dome. The petroclinoidal dural fold was depicted at the inferoposterior aspect of the dome. The anteromedial margin of the temporal lobe showed contact with the superoposterior aspect of the dome. The 3D MR angiogram (Fig 1*E*), coordinated projection as to the 3D MR cisternogram in Figure 1*D*, showed the aneurysm with 3 blebs. The fusion image of 3D MR cisternography and MR angiography (Fig 1*F*), a composite image of the 3D MR cisternography (Fig 1*D*) and MR angiography (Fig 1*E*), revealed the spatial relationship of the dome blebs to the adjacent structures: concavity of the medial aspect of the dome related to the obstacles composed of the posterior clinoid process as a mold and the posteroinferior blebs related to the intermediated petroclinoidal dural fold.

Case 3: Unruptured Internal Carotid-Posterior Communicating Artery Aneurysm (Fig 2)

A 60-year-old man had a left internal carotid-posterior communicating artery aneurysm. The operative photograph (Fig 2*A*) showed the caudal view of the left superolateral aspect of the aneurysmal complex and perianeurysmal structures, including the aneurysm, internal carotid artery, the left optic nerve, and cranial base bone. The digital subtraction angiogram (Fig 2*B*), right lateral projection, showed the aneurysm. The serial source axial images of MR cisternography (Fig 2*C*), superoinferior projection, depicted the aneurysmal complex, left oculomotor nerve, posterior clinoid process and dorsum sellae, and the adjacent temporal lobe. The 3D MR cisternogram (Fig 2*D*), right posterolateral projection and viewed from the basal cistern, showed the spatial relationship and contact of the aneurysm with the perianeurysmal structures. The left oculomotor nerve ran toward the medial aspect of the dome then turned in a superoposterior direction over the dome, but the nerve was disrupted partially by the motion artifact. The posterior aspect of the dome came in contact with the anteromedial margin of the temporal lobe. The 3D MR angiogram (Fig 2*E*), coordinated projection as to the 3D MR cisternogram in Figure 2*D*, showed the aneurysm with a bleb. The fusion image (Fig 2*F*), coordinated projection as to the 3D MR cisternogram in Figure 2*D*, revealed the spatial relationship of the dome bleb to the adjacent oculomotor nerve; protrusion on the medial aspect of the dome showed firm contact with the confronting oculomotor nerve. Postoperatively, the patient showed transient left oculomotor nerve palsy, though the relationship of the inferomedial aspect of the dome to the left oculomotor nerve was not confirmed directly during microneurosurgery.

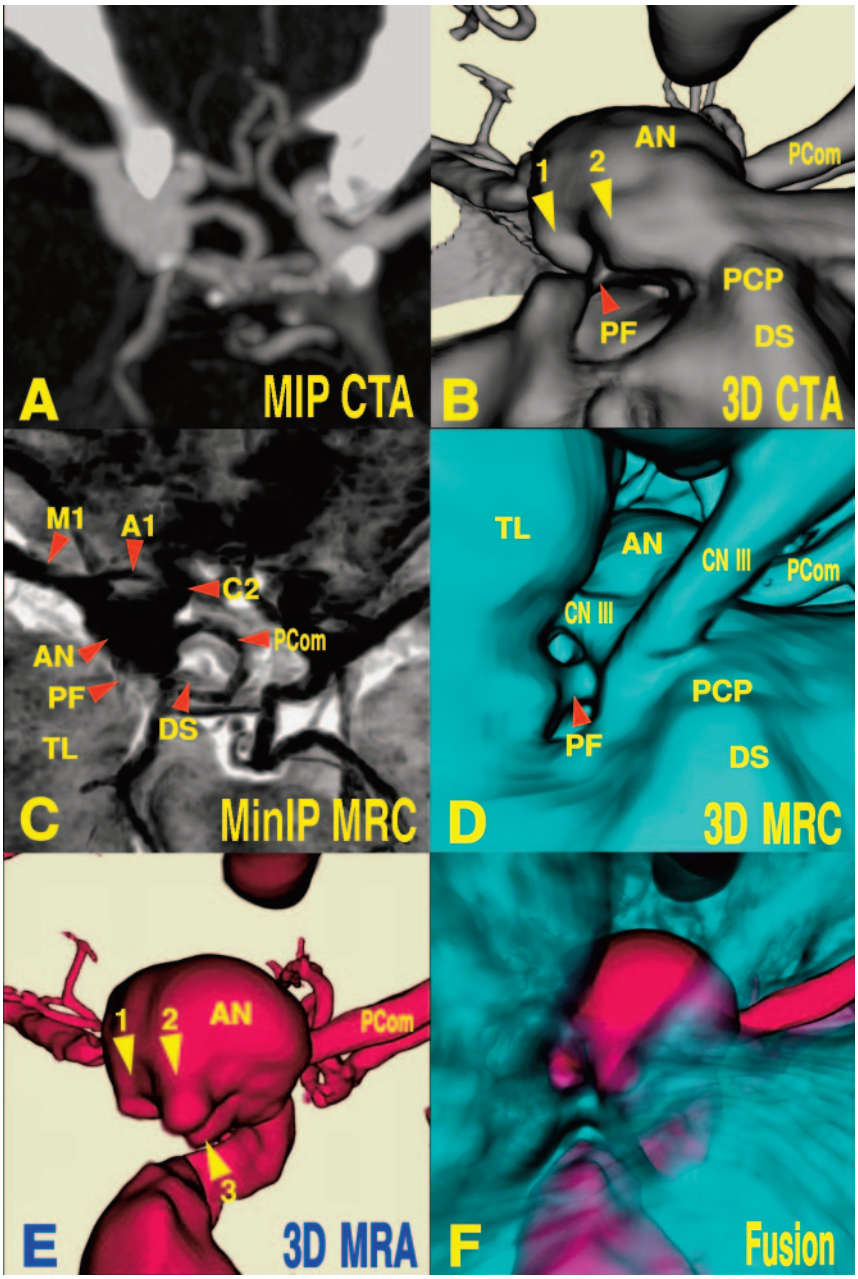

FIG 1. Case 1, a 75-year-old woman with an unruptured internal carotid-posterior communicating artery aneurysm.

A, Maximum intensity projection (MIP) image of the source CT angiography (CTA), superoinferior projection, shows aneurysmal complex and cranial base bone.

B, 3D CT angiogram (CTA), posteroanterior projection, shows the aneurysm (AN), posterior communicating artery (PCom), posterior clinoid process (PCP), dorsum sellae (DS), and petroclinoidal dural fold (PF). Arrowheads (1, 2) indicate the blebs.

C, Minimum intensity projection (MinIP) image of the MR cisternography (MRC), superoinferior projection, shows the aneurysm (AN) and perianeurysmal structures. A1 indicates the first segment of the anterior cerebral artery; M1, the first segment of the middle cerebral artery; C2, the second segment of the internal carotid artery; PCom, posterior communicating artery; PCP, posterior clinoid process; DS, dorsum sellae; PF, petroclinoidal dural fold; TL, temporal lobe.

D, 3D MRC, similar projection to 3D CTA in *B,* viewed from the basal cistern, shows the spatial expansion and contact of the aneurysm with the perianeurysmal structures. CN III indicates oculomotor nerve.

E, 3D MR angiogram (MRA), coordinated projection as to the 3D MRC in *D,* shows the aneurysm with 3 blebs (arrowheads 1–3).

F, Fusion image of the 3D MRC and MRA coordinated projection as to the 3D MRC in *D* shows the spatial relationship of the dome blebs to the adjacent structures.

Case 7: Unruptured Anterior Communicating Artery Aneurysm (Fig 3)

A 76-year-old-woman had an anterior communicating artery aneurysm. The minimum intensity projection images of the source MR cisternogram (Fig 3*A*), superoinferior projection, showed the aneurysmal complex and perianeurysmal structures. The 3D MR cisternogram (Fig 3*B*), anteroinferoposterior projection and viewed from the bottom of the basal cistern, showed the spatial relationship and firm contact of the aneurysm with the optic nerves and the anterior portion of the chiasm. The 3D MR angiogram (Fig 3*C*), coordinated projection as to the 3D MR cisternogram in Figure 3*B*, showed the aneurysm with deformed dome and a bleb. The fusion image (Fig 3*D*) depicted the spatial relationship of the dome to the adjacent optic nerves and chiasm; the inferoposterior portion of the dome was embedded into the chiasm. Deformation of the dome (crest) could be induced by the obstacle of the adjacent chiasm as a mold. A bleb projecting off the left anterolateral projection along the left optic nerve might not be affected by the optic nerve directly. Alternations in intraaneurysmal flow caused by the deformation of the dome may induce the left-sided bleb formation.

Case 8: Unruptured Middle Cerebral Artery Aneurysm (Fig 4)

A 67-year-old-woman had a right middle cerebral artery aneurysm. The digital subtraction angiogram (Fig 4*A*), anteroposterior projection, showed the aneurysm and parent arteries. By reviewing the source axial and reconstructed coronal images of MR cister-

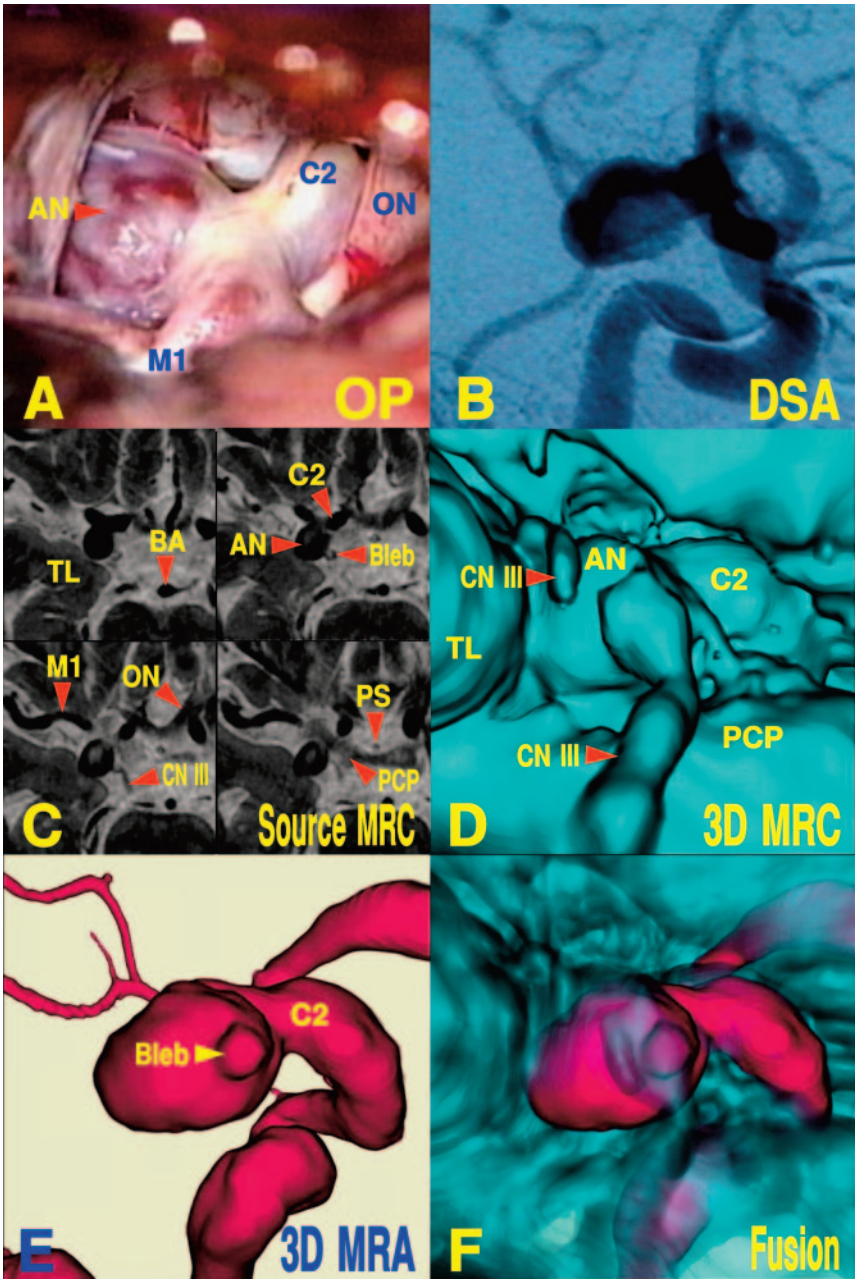

FIG 2. Case 3, a 60-year-old man with an unruptured internal carotid-posterior communicating artery aneurysm.

A, Operative photograph (OP), caudal view, shows the aneurysm (AN). C2 indicates the second portion of the internal carotid artery; M1, first segment of the middle cerebral artery; ON, optic nerve.

B, Digital subtraction angiogram (DSA) is in right lateral projection.

C, Serial source images of MR cisternography (MRC), superoinferior projection, show aneurysmal complex and perianeurysmal structures. BA indicates the basilar artery; TL, temporal lobe; M1, first segment of the middle cerebral artery; ON, optic nerve; PS, pituitary stalk; CN III, oculomotor nerve; AN, aneurysm; C2, second segment of the internal carotid artery; PCP, posterior clinoid process.

D, 3D MRC, right posterolateral projection, is viewed from the basal cistern. CN III indicates oculomotor nerve; TL, temporal lobe; AN, aneurysm; C2, second segment of the internal carotid artery; PCP, posterior clinoid process.

E, 3D MR angiogram (MRA), coordinated projection as to the 3D MRC in *D,* shows the aneurysm with a bleb (*arrowhead*).

F, Fusion image of the 3D MRC and MRA shows spatial relationship of the dome bleb to the adjacent oculomotor nerve.

nography (Fig 4*B*, -*C*), we discriminated the aneurysmal complex from the surrounding superficial veins by their running courses and histograms of MR signal-intensity distribution. Figure 4*C* shows a view position for the 3D MR cisternogram shown in Figure 4D. The 3D MR cisternogram (Fig 4*D*), left anteroinferoposterior projection and viewed from the sphenoidal compartment of the deep sylvian fissure, showed the spatial relationship of the aneurysmal complex to the perianeurysmal structures, including the temporal lobe and superficial middle cerebral veins draining into the sphenoparietal sinus. The 3D MR angiogram (Fig 4*E*), coordinated projection as to the 3D MR cisternogram in Figure 4*C*, showed the arterial components of the aneurysmal complex. The fusion image (Fig 4*F*) revealed the relationship of the dome to the adjacent brain and veins; part of the dome showed contact with the adjacent temporal lobe. Bridging and surface sylvian veins ran beneath the proximal aneurysmal neck.

Case 12: Unruptured Basilar Artery Top Aneurysm Resulting in Rupture (Fig 5)

A 70-year-old-woman had a basilar artery top aneurysm that resulted in a fatal subarachnoid hemorrhage due to aneurysmal rupture in the next 14 months. The 3D CT angiogram (Fig 5*A*), posteroanterior projection, showed the aneurysm and cranial base bone. The 3D MR cisternogram (Fig 5*B*), posteroanterior projection viewed from the interpeduncular cistern, showed the spatial relationship of the aneurysm with the dome, bleb, parent arteries, and caudal aspect of the diencephalon. The 3D MR an-

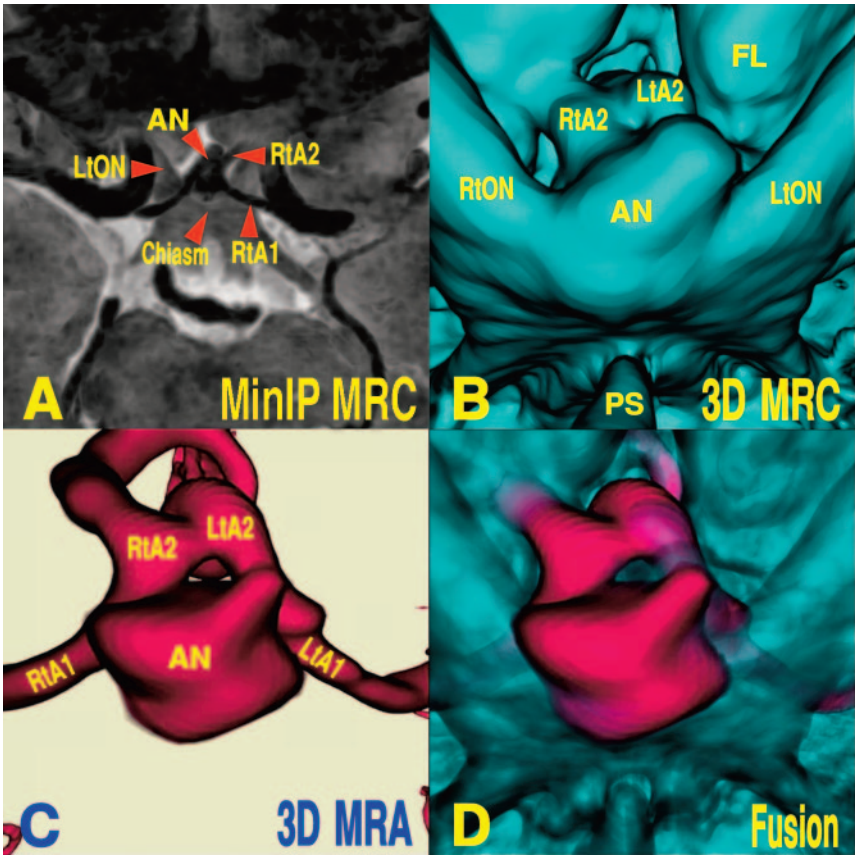

FIG 3. Case 7, a 76-year-old woman with an unruptured anterior communicating artery aneurysm.

A, Minimum intensity projection (MinIP) image of MR cisternography (MRC), superoinferior projection, shows the aneurysm (AN) and perianeurysmal structures. RtA2 indicates the second segment of the right anterior cerebral artery; Chiasm, optic chiasm; RtA1, first segment of the right anterior cerebral artery; LtON, left optic nerve.

B, 3D MRC, inferosuperoposterior projection, viewed from the bottom of the basal cistern, shows the firm contact of the aneurysm with the optic nerves and chiasm. RtA2, second segment of the right anterior cerebral artery; LtA2, second segment of the left anterior cerebral artery; RtON, right optic nerve; LtON, left optic nerve; FL, frontal lobe; PS, pituitary stalk.

C, 3D MR angiogram (MRA), coordinated projection as to the 3D MRC in *B,* shows the aneurysm with deformed dome and a bleb. LtA1 indicates the first segment of the left anterior cerebral artery; LtA2, second segment of the left anterior cerebral artery; RtA1, first segment of the right anterior cerebral artery; RtA2, second segment of the right anterior cerebral artery.

D, Fusion image of the 3D MRC and MRA shows the spatial relationship of the dome to the adjacent optic nerves and chiasm.

giogram (Fig 5*C*), coordinated projection as to the 3D MR cisternogram in Figure 5*B*, showed the arterial components of the aneurysmal complex. The fusion image (Fig 5*D*) depicted the spatial relationship of the dome to the adjacent brain; the tip of the dome bleb extended to the right anterolateral projection and contacted the floor of the third ventricle (diencephalon).

Discussion

Surface irregularity, deformation, bleb formation, and multilobe configuration appearing on the dome of relatively large unruptured cerebral aneurysms can be a morphologic sign indicating a tendency to rupture (2–8). However, the precise mechanism for change in the shape of the aneurysm is not known. Is it influenced by wall shear stress due to intraaneurysmal hemodynamics alone, or by the perianeurysmal environment, or by the combination of the complex and complicated intrinsic and extrinsic factors?

Initiation, subsequent growth, and rupture of a cerebral aneurysm are considered to be influenced mainly by hemodynamic stress related to arterial pressure, pulsatility, and blood flow (11–18). In the geometrically realistic acrylic models for aneurysms harboring blebs, Tateshima et al (15) found that the aneurysmal dome blebs were exposed to higher fluid-induced shear stress than any other measured points on the aneurysmal wall. The bleb might be formed at the portion exposed to high wall shear stress, or the bleb might induce a higher shearing velocity within the dome that results in increased wall shear stress. Additionally, Hassan et al (17) reconstructed computational replicas from the volume data obtained by the 3D digital subtraction angiography and simulated intraaneurysmal blood flow. The ruptured areas of the aneurysms were correlated with areas of high wall shear stress that was induced by the bloodstream turning along the aneurysmal wall in a large area around the localized high-pressure spot. In a case with multiple blebs on the dome, the largest bleb in the low shear stress area was not ruptured, but dome blebs in the high shear stress area were ruptured. Because persistent high wall shear stress might cause local dilation and degeneration of arterial walls, focal increase in fluid-induced wall shear stress was considered as a major factor inducing morphologic change of the aneurysmal dome.

In contrast, shape or geometry of an aneurysm may affect intraaneurysmal hemodynamics. As for the fundamental patterns of intraaneurysmal flow composed of inflow, circulating flow, and outflow, Ujiie et al (14) found the circulating flow depended on the aspect ratio (aneurysmal depth/neck width). A localized, extremely low-flow condition or stagnant flow was commonly observed within the dome of aneurysms with aspect ratios of more than 1.6; moreover, the above-flow pattern was characteristic in the geometry of ruptured aneurysms. Localized stagnation of intraaneurysmal flow might induce degeneration and fragility of the aneurysmal wall and then produce

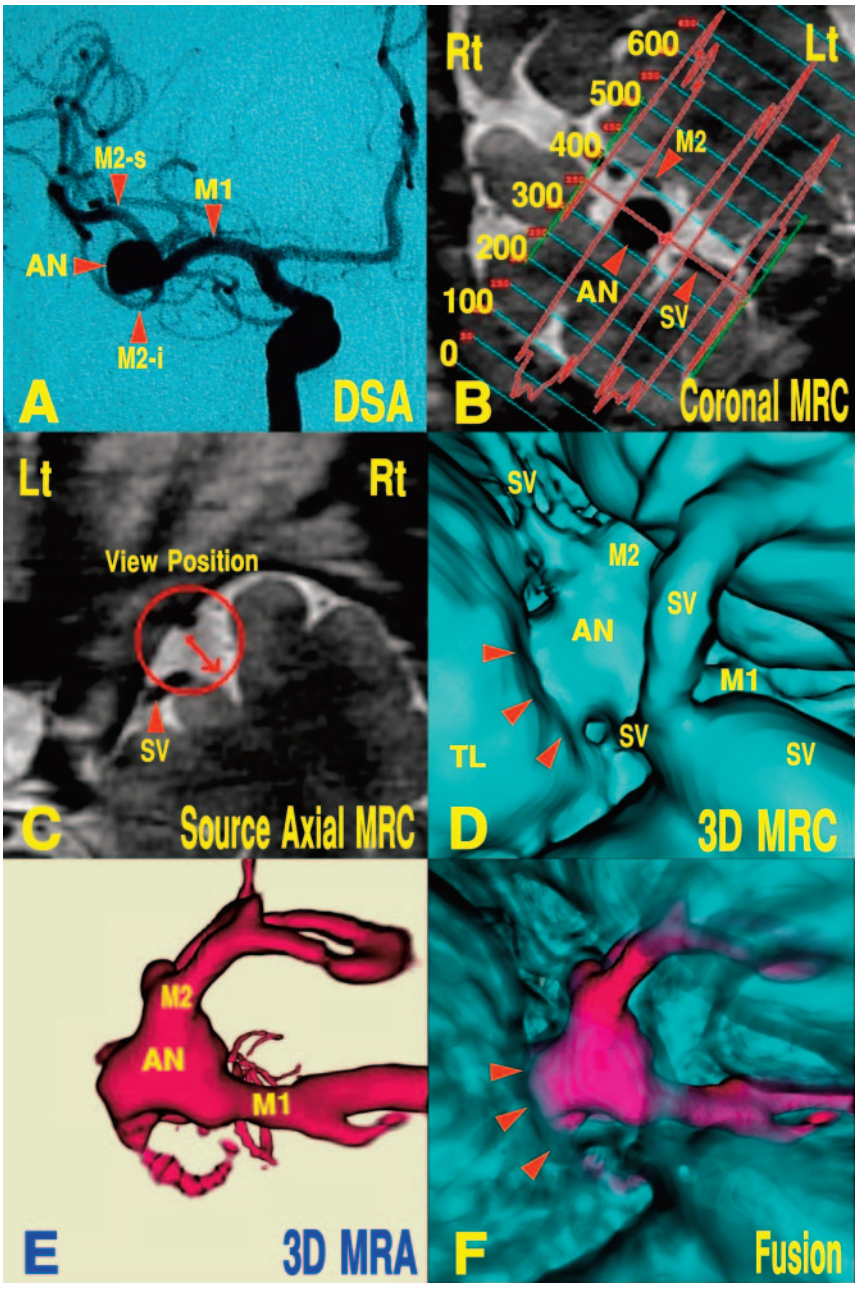

FIG 4. Case 8, a 67-year-old-woman with a middle cerebral artery aneurysm.

A, Digital subtraction angiogram (DSA), anteroposterior projection, shows the aneurysm (AN) and parent arteries. M2-s indicates the superior branch of the second segment of the right middle cerebral artery; M2-i, inferior branch of the right middle cerebral artery; M1, the first segment of the middle cerebral artery.

B, Reconstructed coronal image of MR cisternography (MRC) with MR signal intensity histogram shows the aneurysmal complex and surrounding superficial veins. AN indicates aneurysm; M2, second segment of the middle cerebral artery; SV, superficial middle cerebral veins.

C, Source axial image of MRC, superoinferior projection, shows a view position (*encircled arrow*) for 3D MRC in *D.* SV indicates superficial middle cerebral vein.

D, 3D MRC, left anteroinferior projection, viewed from the sphenoidal compartment of the deep sylvian fissure as indicated in *C,* shows the spatial relationship of the aneurysm (AN), temporal lobe (TL), and superficial middle cerebral veins (SV). Arrowheads indicate contact of the dome with the adjacent temporal lobe; M1, first segment of the middle cerebral artery; M2, second segment of the middle cerebral artery.

E, 3D MR angiogram (MRA), coordinated projection as to the 3D MRC in *D,* shows the arterial components of the aneurysmal complex.

F, Fusion image of the 3D MRC and MRA shows a part of the dome contact with the adjacent temporal lobe (*arrowheads*).

a dome bleb, resulting in rupture, even with physiologic tensile forces.

However, no mention has been made of the extrinsic factors affecting morphologic change in shape with growth and enlargement of an aneurysm. The perianeurysmal environment may be a factor inducing deformation and bleb formation of the aneurysmal dome owing to the anatomic limitation in spatial expansion (19, 20). Because the perianeurysmal environment varies according to the anatomic space composed of intra- and juxtacisternal structures in which the aneurysm develops and grows, size and shape of each individual aneurysm may be affected by its own perianeurysmal environment. Assessment of the anatomic spatial relationship between the aneurysmal complex and the perianeurysmal environment may provide useful information in consideration of growth and expansion of the aneurysm, development of cranial nerve symptoms, deformation and bleb formation of the dome, and potential risk of rupture (20).

MR cisternography depicts the vascular structures, including vessels and aneurysms, with profoundly low signal intensity; cranial nerves and brain parenchyma with moderately low signal intensity; and cranial base bones with variable signal intensities (20–22). Thus, the space-occupying intra- and juxtacisternal structures are well demarcated by the profoundly hyperintense adjacent subarachnoid cerebrospinal fluid. The 3D reconstruction of those cisternographic volume data with a perspective volume-rendering algorithm can depict the spatial relationship between the intra- and juxtacisternal structures and the aneurysm that develops within the corresponding cerebrospinal fluid space (20). In addition, MR angiography ob-

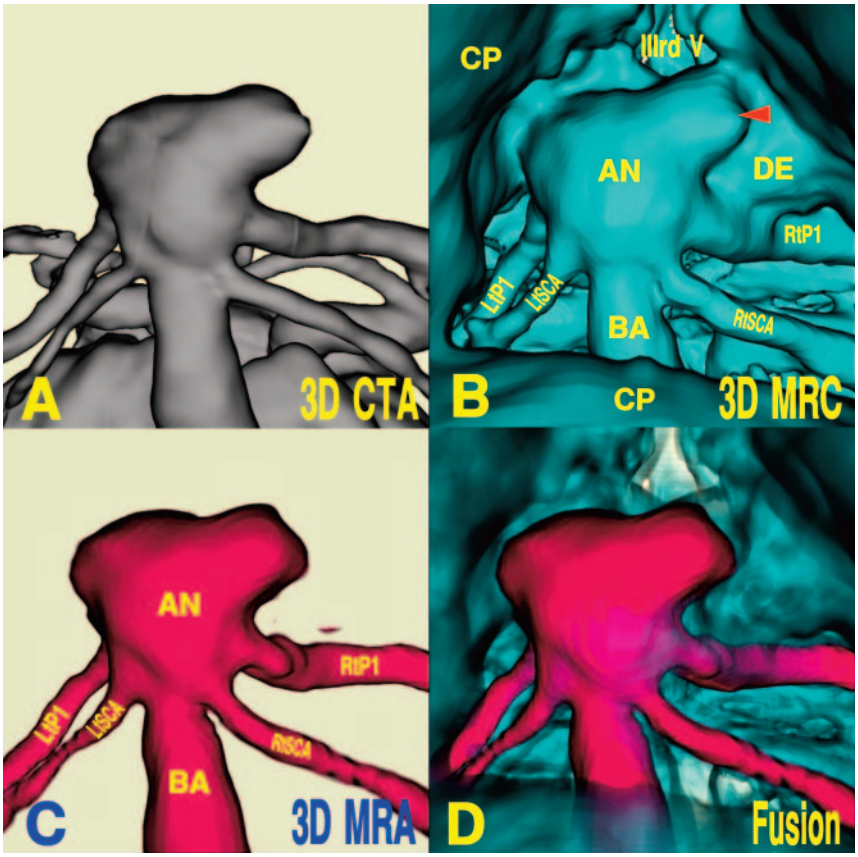

FIG 5. Case 12, a 70-year-old-woman with a basilar artery top aneurysm resulting in rupture.

A, 3D CT angiogram (CTA), posteroanterior projection, shows the aneurysm and cranial base bone.

B, 3D MR cisternogram (MRC), posteroanterior projection viewed from the interpeduncular cistern, shows the spatial relationship of the aneurysm with dome blebs, parent arteries, and caudal aspect of the diencephalon and the third ventricle. DE indicates diencephalon; IIIrd V, the third ventricle; CP, cerebral peduncle; LtP1, first segment of the left posterior cerebral artery; RtP1, first segment of the right posterior cerebral artery; LtSCA, left superior cerebellar artery; RtSCA, right superior cerebellar artery; BA, basilar artery. Arrowhead indicates the bleb.

C, 3D MR angiogram (MRA), coordinated projection as to the 3D MRC in *B,* shows the arterial components of the aneurysmal complex.

D, Fusion image of the 3D MRC and MRA shows the contact of the dome bleb with the floor of the adjacent third ventricle (diencephalon).

tained by the 3D time-of-flight sequence shows not the vascular morphology but inflow effect related mainly to peak inflow velocity within the vessel lumen during the data acquisition process through the diastolic and systolic cardiac cycle (6, 7). With use of a 3D MR cisternography–MR angiography fusion image, vascular structures depicted on the 3D MR cisternogram can be discriminated by referencing the coordinated 3D MR angiogram; this fusion imaging technique can provide an assessment of the contact between cerebral aneurysms and anatomic elements of their perianeurysmal environments.

In the present study, contact between an aneurysm and the perianeurysmal environment was assessed on the 3D MR cisternography–MR angiography fusion images. When the internal carotid-posterior communicating artery aneurysm extended posteroinferiorly (case 1), then the aneurysmal dome came into contact with surrounding hard structures such as the tentorial free edge, petroclinoidal dural fold, and posterior clinoid process, and marked deformation was observed on the dome. This deformation was consistent with multilobe configurations composed of multiple dome blebs depicted by 3D MR angiography. In cases in which the aneurysms grew in size and contacted adjacent soft tissues (cases 3, 7, 8, 12), including brain parenchyma (temporal and frontal lobes, brain stem, diencephalon) and cranial nerves (optic nerve, optic chiasm, oculomotor nerve), minor deformation was usually depicted. However, when the aneurysms expanded toward the brain (cases 8, 12), dome and bleb were protruded and embedded within the brain parenchyma. In a specific case of internal carotid-posterior communicating artery aneurysm resulting in transient oculomotor nerve palsy postoperatively (case 3), the dome extended posteromedially and might have been in adhesive contact with the oculomotor nerve, where a dome bleb was formed in the corresponding location. These results suggest that deformation and bleb formation of the aneurysmal dome were found at the areas confronted or adjacent to a certain contact with perianeurysmal structures. When the aneurysm increases in size beyond the capacity of the surrounding subarachnoid space, morphologic change in the aneurysmal shape may be affected by the contact with the perianeurysmal environment. Deformation and bleb formation on the aneurysmal dome may not be influenced by the surrounding structures alone, but by the complex and complicated interaction between hemodynamics, pathologic factors, and the perianeurysmal environment.

Conclusion

Several factors and complex mechanisms may affect the initiation, growth, and rupture of cerebral aneurysms. A perianeurysmal environment composed of the intra- and pericisternal anatomic structures may play an important role in inducing deformation and bleb formation of an unruptured cerebral aneurysm, when its size exceeds the capacity of the sur-

rounding subarachnoid space. The 3D MR cisternography–MR angiography fusion imaging can depict the contact of an aneurysm with its perianeurysmal environment; this may provide an additional parameter in the consideration of the natural history of a cerebral aneurysm, especially for the development of cranial nerve symptoms and production of a dome bleb leading to leakage or rupture. Further study is required to elucidate a causal relationship between the perianeurysmal environment and aneurysm development.

References

1. Rhoton AL Jr. Aneurysms. *Neurosurgery* 2002;51[suppl 1]:121–158
2. Crompton MR. **Mechanism of growth and rupture in cerebral berry aneurysms.** *BMJ* 1966;1:1138–1142
3. Weibers DO, Whisnant JP, Sundt TM Jr, et al. **The significance of unruptured intracranial saccular aneurysms.** *J Neurosurg* 1987;66:23–29
4. Asari S, Ohmoto T. **Natural history and risk factors of unruptured cerebral aneurysms.** *Clin Neurol Neurosurg* 1993;95:205–214
5. Hademenos GJ, Massoud TF, Turjman F, et al. **Anatomical and morphological factors correlating with rupture of intracranial aneurysms in patients referred for endovascular treatment.** *Neuroradiology* 1998;40:755–760
6. Satoh T, Onoda K, Tsuchimoto S. **Visualization of intraaneurysmal flow patterns with transluminal flow imaging of three-dimensional MR angiograms in conjunction with aneurysmal configurations.** *AJNR Am J Neuroradiol* 2003;24:1436–1445
7. Satoh T, Ekino C, Ohsako C: **Transluminal color-coded three-dimensional magnetic resonance angiography for visualization of signal intensity distribution pattern within an unruptured cerebral aneurysm: preliminarily assessment with anterior communicating artery aneurysms.** *Neuroradiology* 2004;46:628–634
8. Rohde S, Lahmann K, Beck J, et al. **Fourier analysis of intracranial aneurysms: towards an objective and quantitative evaluation of the shape of aneurysms.** *Neuroradiology*. 2005;47:121–126. Epub 2005 Feb 2
9. Kataoka K, Taneda M, Asai T, et al. **Structural fragility and inflammatory response of ruptured cerebral aneurysms: a comparative study between ruptured and unruptured cerebral aneurysms.** *Stroke* 1999;30:1396–1401
10. Frösen J, Piippo A, Paetau A, et al. **Remodeling of saccular cerebral artery aneurysm wall is associated with rupture**: **histological analysis of 24 unruptured and 42 ruptured cases.** *Stroke* 2004;35:2287–2293
11. Gonzalez CF, Cho YI, Ortega HV, et al. **Intracranial aneurysms: flow analysis of their origin and progression.** *AJNR Am J Neuroradiol* 1992;13:181–188
12. Kerber CW, Liepsch D. **Flow dynamics for radiologists. II. Practical considerations in the live human.** *AJNR Am J Neuroradiol* 1994;15:1076–1086
13. Burleson AC, Strother CM, Turitto VT. **Computer modeling of intracranial saccular and lateral aneurysms for the study of their hemodynamics.** *Neurosurgery* 1995;37:774–784
14. Ujiie H, Tachibana H, Hiramatsu O, et al. **Effects of size and shape (aspect ratio) on the hemodynamics of saccular aneurysms: a possible index for surgical treatment of intracranial aneurysms.** *Neurosurgery* 1999;45:119–130
15. Tateshima S, Murayama Y, Villablanca JP, et al. **In vitro measurement of fluid-induced wall shear stress in unruptured cerebral aneurysms harboring blebs.** *Stroke* 2003;34:187–192
16. Steinman DA, Milner JS, Noreley CJ, et al. **Image-based computational simulation of flow dynamics in a giant intracranial aneurysm.** *AJNR Am J Neuroradiol* 2003;24:567–578
17. Hassan T, Timofeev EV, Saito T, et al. **Computational replicas: anatomic reconstructions of cerebral vessels as volume numerical grids at three-dimensional angiography.** *AJNR Am J Neuroradiol* 2004;25:1356–1365
18. Shojima M, Oshima M, Takagi K, et al. **Magnitude and role of wall shear stress on cerebral aneurysm: computational fluid dynamic study of 20 middle cerebral artery aneurysms.** *Stroke* 2004;35:2500–2505
19. Ruiz DSM, Tokunaga K, Dehdashti AR, et al. **Is the rupture of cerebral berry aneurysms influenced by the perianeurysmal environment?** *Acta Neurochir Suppl* 2002;82:31–34
20. Satoh T, Omi M, Ohsako C, et al. **Visualization of aneurysmal contours and perianeurysmal environment with conventional and transparent 3D MR cisternography.** *AJNR Am J Neuroradiol* 2005;26:313–318
21. Rubinstein D, Sandberg EJ, Breeze RE, et al. **T2-weighted three-dimensional turbo spin-echo MR of intracranial aneurysms.** *AJNR Am J Neuroradiol* 1997;18:1939–1943
22. Mamata Y, Muro I, Matsumae M, et al. **Magnetic resonance cisternography for visualization of intracranial fine structures.** *J Neurosurg* 1998;88:670–678